Article

Coupled Meteo–Hydrodynamic Approach in Semi-Enclosed Basins and Sensitivity Assessment of Wind-Driven Current

Elvira Armenio [1,*], Andrea Tateo [1], Francesca Fedele [1], Nicola Ungaro [1], Michele Mossa [2], Vittorio Esposito [1] and Vincenzo Campanaro [1]

1　Apulia Region Environmental Protection Agency (ARPA Puglia), C.so Trieste 27, 70126 Bari, Italy;
　a.tateo@arpa.puglia.it (A.T.); f.fedele@arpa.puglia.it (F.F.); n.ungaro@arpa.puglia.it (N.U.);
　v.esposito@arpa.puglia.it (V.E.); v.campanaro@arpa.puglia.it (V.C.)
2　Department of Civil, Environmental, Building Engineering and Chemistry (DICATECh), Polytechnic
　University of Bari, 70126 Bari, Italy; michele.mossa@poliba.it
*　Correspondence: e.armenio@arpa.puglia.it

Abstract: A coupled numerical approach that combines the WRF model and the Mike 3 (DHI) hydrodynamic model was developed and applied in two semi-enclosed basins in the Ionian Sea (Italy) to assess the wind-driven current. To gain a better understanding of how the sea current field can vary depending on meteorological data forcing, three different scenario were set up. The sensitivity of the sea current pattern was investigated as a function of the type of meteorological forcing and appreciating the differences in the results. The aims of this study are threefold. Firstly, we wish to define an ad hoc procedure to join the model-computed meteorological parameters in the hydrodynamic model. Secondly, we will investigate the feedback from the Mar Piccolo and Mar Grande basins in the Ionian Sea using fully coupled simulations and an uncoupled system where the atmospheric parameters are derived from a ground station. Finally, we will evaluate the results achieved by applying two scenarios of typical meteorological conditions to the study site. The model results highlighted the variability of sea currents depending on meteorological forcing.

Keywords: environmental monitoring; hydrodynamics; meteorological model

1. Introduction

Coastal basins are the location of important ecosystem services, such as fishing, aquaculture and tourism. Many manufacturing activities occur not far from the coast for needs such as the transport of raw materials and finished products. Over the 20th century, population growth, urbanization, and anthropogenic development have caused the alteration of coastal processes and thus the provision of these services. From the scenario outlined, it follows that coastal zones over the years have been exposed to the continuous action of numerous factors, both natural and human-induced, operating on different time scales. Coastal basins are vulnerable environments to both natural and human-induced hazards. Therefore, in-depth knowledge is needed to assess their evolution and resilience. Furthermore, appropriate protection and conservation efforts need to be devised to tackle the environmental impacts of human works and adaptation to climate change [1]. A comprehensive knowledge of coastal basins is the primary basis for any management plan and decision-making. In fulfillment of this demand, in recent decades, regulatory bodies have commissioned multi-year monitoring programs to investigate in situ environmental parameters. Examples are the monitoring programs implemented at the regional scale to monitor the quality of the most relevant basins [2]. Nevertheless, classic monitoring systems often entail the use of instrumentation to measure the characteristics of a basin at point level (e.g., sampling, use of multi-parameter probes to determine physical–chemical parameters, velocimeter to detect the current velocity and direction along the water column). Hence, time-varying series referring to the measurement point are derived [3].

From the above considerations, it is evident that the simple use of in situ monitoring does not guarantee to achieve in-depth knowledge of a coastal basin. Numerical models can also help meet this need [4]. Nowadays, developments in the field of numerical codes have provided advanced and reliable tools capable of providing a thorough understanding of the spatial and/or temporal evolution of the most important environmental parameters [5]. Modern modeling systems can be used to scale from the ocean to the coastal scale, and the recent trend is to develop multi-scale modeling systems based on a multiple-nesting approach [2,6]. In general, numerical models, appropriately validated with in situ measurements, allow us to reproduce and predict marine physical processes relatively quickly, accurately and at a moderate cost. Operational oceanography commonly uses models covering regional, sub-regional and coastal scales [7,8]. To study local scales, with a resolution of a few hundred meters, multi-scale modeling systems based on a multiple-nesting approach have recently been successfully implemented [9]. Furthermore, numerical models are capable of supporting environmental decision-making by simulating scenarios resulting from human activities.

Several numerical hydrodynamic studies applied in coastal basins are available in the literature in which the wind forcing is considered as a time series. More information can be found in [3,5]. Sometimes, the meteorological forcing was obtained through the use of a specific meteorological model, as in this study [1]. Nevertheless, no specific studies were carried out to evaluate the coupling of a hydrodynamic model with a meteorological model. Despite the availability of high-performance numerical models, it is still a challenge to obtain the most accurate and faithful representation of a site. The joint use of several advanced numerical models can be a key point to this scope [10,11].

To this end, this study aims to combine two numerical models, a meteorological and a hydrodynamic model, respectively. We used the Weather Research and Forecasting (WRF) model [12] coupled with the Danish Hydraulic Institute (DHI) Mike 3 hydrodynamic model [13]. In our Agency, we use the WRF model, an open-source code, as input for the air quality model. On the other hand, DHI's Mike is a commercial code that allows modeling water circulation in 3D for rivers, lakes, coastal and offshore marine waters. A dedicated operating procedure was set up to couple the two models in an attempt to use the data generated as output of the WRF model inside the modeling developed with the Mike 3 hydrodynamic model. In particular, we aimed to investigate the sensitivity of the sea current pattern as a function of the type of meteorological forcing applied and gain a better understanding of how the sea current field can vary depending on meteorological data forcing. To appreciate the joint use of the numerical model, we tested it in a case study. Especially, a hydrodynamic modeling application was carried out in a vulnerable and heavily man-made semi-enclosed basin called Mar Piccolo located in the city of Taranto, southern Italy [14,15]. Moreover, the site is also located close to an industrial area. The present paper falls within the scope of the activities carried out by the authors in terms of marine monitoring (see, for example, [1–3]).

Previous studies [9,11] applied numerical model simulation to that area to investigate the dynamics of current circulation in the semi-enclosed basin. However, less attention was paid to the susceptibility of surface circulation currents than to the variability of wind forcing. The implemented procedure is therefore innovative for the study site. This paper aims to show how the joint use of numerical models in a semi-enclosed sea can be managed to quickly provide fundamental insights into its hydrodynamic structure and environmental health. This straightforward and replicable procedure has been applied with good results [1–3], interesting from a predictive and numerical modeling perspective [7,10]. Even though typical circulation and water exchange trends have been studied by several models developed for the Taranto Sea, further observations, monitoring actions and numerical modeling are still needed to better understand the most significant hydrodynamic–biological variability in this coastal basin. The results of this study can be applied to similar areas. Furthermore, it has proved to be a necessary tool for local authorities and stakeholders, enabling them to gain a deeper understanding of the site. The

present study is aimed toward the evaluation of the model for possible future operational use. The paper is organized as follows. In Section 2, the methodological approach adopted and a description of the study area are outlined. The different numerical simulations are described in Section 3. Results and discussion are presented in Section 4, while conclusions cover Section 5.

2. Materials and Methods

2.1. Methodological Approach

We aimed to investigate the sensitivity of the sea current pattern as a function of the type of meteorological forcing applied and gain a better understanding of how the sea current field can vary depending on meteorological data forcing. The objective will be addressed through the simulation of forced current circulations from time-series meteorological data, temporal and spatial variability data and no meteorological data. To this end, we set up a hydrodynamic simulation on a coastal basin by running various scenario configurations of wind data and appreciating the differences in the results. For the hydrodynamic modeling to simulate circulation currents, and thus water movement, several forcing factors are involved. Among these, a fundamental role is played by meteorological data including, in particular, wind speed and direction, solar radiation, cloud cover, relative humidity, precipitation, air temperature and atmospheric pressure. Generally, meteorological data are collected from the meteorological stations closest to the study area. In particular, in the present study, we refer to data measured by a single meteorological station. Only time-varying meteorological data (time series) are therefore used for the simulation and assumed constant throughout the domain. Although the representation of the meteorological forcing constitutes a rough approximation, it should also be considered that, in addition, the meteorological station is not always located in the vicinity of the site being hydrodynamically simulated and may even be several kilometers away from the area of interest, which further impairs the representativeness of the meteorological data of the study area. The aims of this study are threefold. Firstly, we wish to define an ad hoc procedure to join the model-computed meteorological parameters in the hydrodynamic model. Secondly, we will investigate the feedback from the Mar Piccolo and Mar Grande basins in the Ionian Sea, using fully coupled simulations and an uncoupled system where the atmospheric parameters are derived from a meteorological station. Finally, we will evaluate the results achieved by applying two scenarios of typical meteorological conditions to the study site.

The methodological approach used was based on the following steps:

- Implement a specific operational procedure for interfacing the WRF model and the Mike circulation model;
- Setting of the hydrodynamic model of the Mar Piccolo basin using the Mike 3 model (DHI);
- Run test of the hydrodynamic model by using as meteorological forcing the data acquired by the closest meteorological station (time-varying data but constant in the domain);
- Run test of the coupled meteo–hydro model by using the meteorological forcing of the output data processed by the WRF model (domain- and time-varying data);
- Comparison and analysis of results obtained for characteristic meteorological conditions.

Figure 1 shows the scheme of the methodological procedure implemented in our study.

2.2. Study Site

The methodological approach defined in the present study was applied in a coastal area located in Southern Italy and composed of two basins embedded in the northern part of the Gulf of Taranto: an inner one called Mar Piccolo and an external one named Mar Grande (Figure 2a,b). Figure 2c shows the computational domain and open boundaries (boundaries: SE in red color and SW in green color). Figure 2d reports the sampling points in the study area named FP01, FP02, PN01, PN02, SV01, SV02. The Mar Piccolo basin, whose area extends around 21.7 km^2, is in turn hydraulically connected to the Mar Grande

basin, a larger one with a surface of approximately 35 km². Mar Grande has a round shape with a maximum water depth of 35 m. Mar Piccolo, in turn, has a particular morphology composed of two circular bays: the I Bay reaches a maximum depth of about 15 m, while in the II Bay, the depth is about 10 m. The I Bay is joined to Mar Grande by two channels: a natural one named the Porta Napoli channel and an artificial one called the Navigable Channel. The Navigable Canal measures 58 m in width, 375 m in length and 14 m in water depth, while the Porta Napoli Canal is 150 m in width and 2.5 m in water depth. The connection between the two bays of the Mar Piccolo basin is provided by an arm of water about 500 m wide between Punta Penna (to the north) and Pizzone (to the south). In antiquity, the two basins represented an important port, and its waters have always been a source of wealth for the people of Taranto, who have practiced profitable fishing and shellfish farming there for centuries [14,15]. In the Taranto area, rainwater, falling on the surrounding Karst-type hills and countryside more or less high above sea level, is rapidly absorbed by the arid soil, filtering through limestone, sandstone, etc. The waters thus reach poorly permeable clay layers and sometimes collect in aquifers located below sea level. From here, finding fractures that are more or less wide and regular, either by pressure or by different densities, rise to the surface originating the so-called citri, springs of fresh or brackish water that have for the Mar Piccolo basin fundamental importance because they act as thermohaline regulators with considerable advantage for shellfish farming activities [16,17]. The natural features of Taranto's Mar Piccolo are mostly referable to those of transitional coastal environments in connection with the open sea, which is characterized by slow water exchange. However, this initial situation was affected over time by a strong anthropogenic (urban and industrial) impact, both on the water body and on the territory adjacent to it, which led to an evident impoverishment of the naturalistic value of the entire area. Because of the Mar Piccolo and Mar Grande complex topography and sedimentation, the hydrodynamic patterns of this basin can only be adequately studied at the local scale. The coastal areas of the Mar Piccolo and Mar Grande basins are used for various activities of anthropogenic nature including shipbuilding activities, the areas occupied by the navy. In addition, the basin is the receptacle of several civil wastewater discharges. Especially, several forcings are located along the coastline of the two basins, including industrial and civil discharges; the mouth of the Galeso, the D'Ajedda Canal and citri (underwater sources) are also present, the most significant of which are Le Copre, Citrello, Galeso and S. Cataldo. Such situations turn this study area into a highly vulnerable one because it is exposed to heavy anthropogenic pressure, urban and industrial discharges, and intense ship traffic [18].
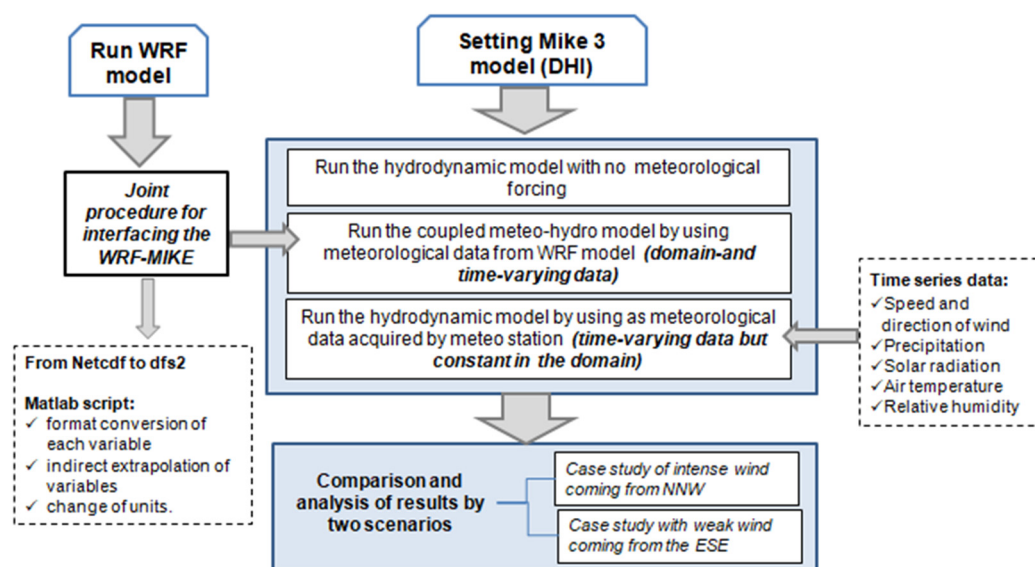

Figure 1. Scheme of the methodological procedure applied. (Source: authors' elaboration).
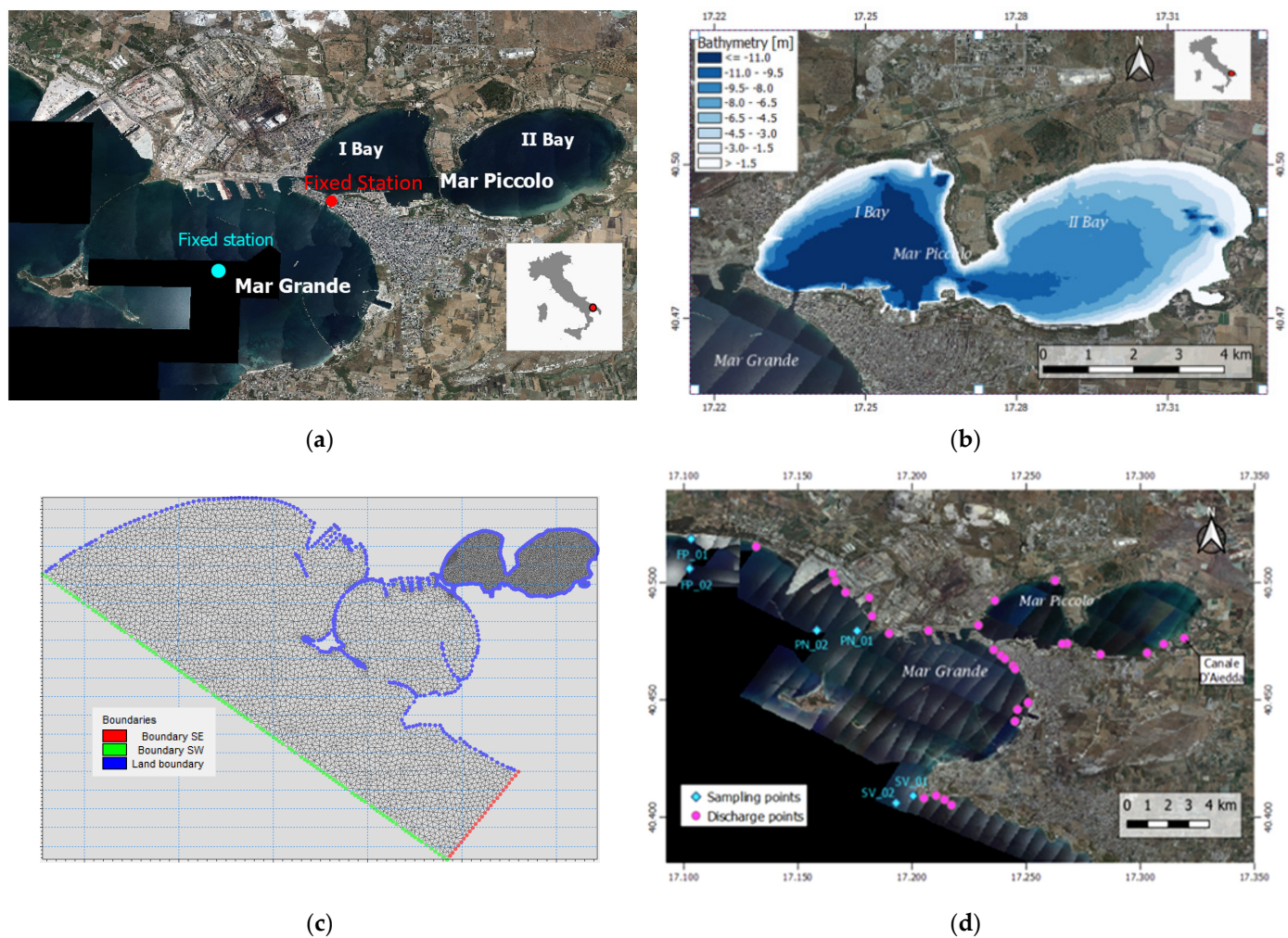
(**a**)

(**b**)

(**c**)

(**d**)

Figure 2. (**a**) Map of Mar Piccolo and Mar Grande; (**b**) Mar Piccolo Basin with a bathymetric map; (**c**) Computational domain and open boundaries (SE in red color and SW in green color); (**d**) Mar Piccolo and Mar Grande basins with the specification of sampling points (marked in light blue) used for fields current measurements and discharge points in the study area (marked in magenta). (Source: authors' elaboration).

2.3. Numerical Simulation

2.3.1. Hydrodynamic Modeling

For the case study described in this paper, the Mike 3 [12] model was applied. This study utilized the Mike 3 Flow Model, which was specified for hydrodynamic modeling but is also suitable for coastal modeling [19,20]. This is due to its flexible mesh capable of co-operating well with asymmetrical coastlines and the combination of vertical sigma-discretization and vertical z-discretization enhances the vertical distribution of the water column and the steep slope of the bathymetry [1]. Through a sigma-type vertical coordinate system, changes in the free surface are taken into account; in addition, the model uses an unstructured computational mesh to ensure the highest degree of flexibility in representing complex geometries [21]. The Mike model is based on the numerical solution of the Navier–Stokes equations averaged over the turbulence period for incompressible 3D flows, assuming that the Boussinesq and hydrostatic assumptions are valid. It, therefore, solves the equations of conservation of mass, momentum, temperature, and salinity and the turbulence closure equation. These characteristics make the numerical model particularly suitable for application to coastal areas such as the one under investigation [22–24]. For the implementation of the model, the computational mesh was first generated. Specifically, a flexible triangular mesh was set up and appropriately infilled at the Navigable Channel

and the connection area between the I and II Bays. Vertical discretization in the model is carried out according to so-called sigma layers, i.e., layers that follow the terrain trend, so that along each vertical a constant number of computation points is obtained. The model domain is composed of unstructured mesh with a low resolution of 500 m in Mar Grande and a finer resolution of 50 m in Mar Piccolo. The model simulation was run for 40 days with 7 days for spinning time. The model was forced by the two sources of bathymetry data which were the European Marine Observation and Data Network (EMODnet portal) and data survey. The unstructured mesh procedure involved domain generation, followed by the natural neighbor interpolation method for bathymetric data and mesh production. Two open boundaries were set in the model: one parallel to the Ionian coast and directed towards the SW and the other, of lesser extent, towards the SE (Figure 2c). The two open boundaries in the domain were initialized with the free-surface elevation time-series data. This is effective to avoid the instability of the open boundary in case of stratified density intrusion, to link the regional-scale model with the local-scale model. The three sets of scenarios were performed for the sensitivity analysis of wind-driven current in Mar Piccolo and Mar Grande waters. The experiments were designed to simulate the meteorological conditions almost without the wind influence (0 m/s), with the extreme wind blowing from NNW and low wind forcing condition blowing from SSE. The experiment was designed to understand the dynamic changes of current circulation patterns under the influence of different types of meteorological data, i.e., time series (time variability and constant in domains) and time–spatial variability. Table 1 summarizes the main features of the simulations considered in this study.

Table 1. Main settings of the hydrodynamic model.

Name	Notation/Comment	Setting
Module Selection	Shallow water equations	Hydrodynamic
Wind drag multiple	constant	0.001255
Run length	days	40
Time step	seconds	3600
Density	barotropic	-
Initial Conditions	Varying in domain	u and v current velocity components [1]
Boundary Conditions	Flather conditions	u and v current velocity components and water level [1]
Eddy viscosity vertical	Log Low Formulation	$0.4 \text{ m}^2/\text{s}$
Eddy viscosity horizontal	Smagorinsky Formulation	0.28
Bed Resistance	Varying in domain	Fields survey
Coriolis forcing	Varying in domain	-

[1] Data from Copernicus Marine Services https://marine.copernicus.eu/ accessed on 30 January 2022.

The main driving forces on the basin, such as tides, winds, inflows, salinity and temperature gradients, were used as input conditions for the numerical runs with the Mike 3 model. The used time-varying water level has been provided by the National Mareographic Network (managed by ISPRA, Institution for Research and Environmental Protection) tide station located at St. Eligius Pier. The Mike model is implemented by downscaling from the Copernicus Marine Service large-scale model, i.e., by entering as open boundaries and initial conditions the data available on the Copernicus portal. Meteorological data from the nearest ARPA Puglia station are used to simulate the meteorological data constant in space and variable in time scenarios. In particular, meteorological data entered into the model include wind speed and direction, precipitation, solar radiation, air temperature, relative humidity, and atmospheric pressure.

2.3.2. Meteorological Modeling

The Weather Research and Forecasting (WRF) model is a mesoscale Numerical Weather Prediction (NWP) model for forecasting the values of weather variables [13].

The term forecasting means both temporal, thereby at instants subsequent to that of execution (forecast), and spatial forecasting, hence at points on planet Earth where there is no meteorological monitoring station (analysis). These types of models provide their output by going numerically to solve the system of nonlinear differential equations governing the atmosphere, something that can be exactly achieved if the initial state is known [25]. For limited area models, the initial state is provided by global models (we use the U.S. GFS model in forecast mode and the ECMWF model in analysis). Since the atmosphere is a nonlinear dynamical system, the solutions of its equations have a strong dependence on the initial conditions, and therefore, variations, however small, in the initial state make the temporal evolution of the system unpredictable (we speak of a deterministic–chaotic system) [26,27]. For the execution of the WRF model, it is necessary to define the characteristics of the global input model (spatial and temporal resolution), the topography to be used (we adopted CORINE appropriately implemented in the WRF model resulting from the previous work [28,29]), the approximations to be considered in solving the differential, the area of interest, the spatial and temporal resolutions, and a whole series of options such as, for example, the type of nesting to be used) [30,31].

The WRF configuration has been investigated in previous and specific studies [30,32,33] very important due to the particular geographical configuration of the Apulia region, a thin strip of land wet on most of its edges from the Adriatic and the Ionian sea. We implemented the WRF simulations in the analysis mode by using as initial and boundary conditions the ECMWF analysis with a spatial resolution of about 16 km and a time resolution of 6 h. We used the WRF model to estimate meteorological parameters on the area of interest with a spatial and temporal resolution of 1 km and 1 h, respectively, by combining the Mellor-Yamada Nakanishi and Niino level 2.5 (MYNN 2.5 level TKE) scheme for the Boundary layer and the Mellor-Yamada Nakanishi and Niino (MYNN) scheme for the Surface layer [34,35]. We performed the WRF model in two distinct output spatial domains: d01 and d02, which have a spatial resolution of 4 and 1 km, respectively. For our analysis, we used the domain with the highest spatial resolution, expecting added value compared to the domain with the lowest resolution [33]. Of all meteorological variables processed by the WRF model, for our purposes, we considered only the two 10 m wind components (U10 and V10), the 2 m air temperature (T2), the 2 m relative humidity (RH2), the precipitation (PREC), the sea surface temperature (SST), the global solar radiation (solar rad.), and the atmospheric pressure (PSFC).

Since not all the variables of our interest are directly provided by the WRF model, we used as post-processing tools the ARWpost algorithms and the Grid Analysis and Display System, (GrADS) based on the nearest-neighbor approach [30,32]. Also, since running a model over large areas and high spatial resolutions (1 km) requires high computational power, the dedicated container has been built in the Docker system available on the data center ReCaS-Bari (https://www.recas-bari.it/) accessed on 1 January 2022, the computing platform that allows running the WRF model with several CPUs up to 200 (currently, the implemented container has been tested with up to 100 CPUs) [34,35].

2.3.3. Coupling of the WRF Meteorological Model with the Hydrodynamic Model

The hydrodynamic modeling implementation is typically performed using available weather data collected from meteorological stations. In the specific case study of this paper/work, weather data recorded by the ARPA Puglia meteorological station were used. Specifically, meteorological data were collected by the ARPA Puglia ground station located in San Vito, a neighborhood of Taranto, part of the monitoring network. The S. Vito station is about 5 km away from the Mar Grande basin and about 8 km away from the Mar Piccolo basin. This station provides 14 distinct measures: minimum, medium, and maximum temperature (°C), minimum, medium, and maximum relative humidity (%), precipitation (mm), mean and maximum 10 m wind speed (m/s), mean 10 m wind direction prevailing 10 m wind direction sector, mean and maximum global radiation (W/m^2), and mean atmospheric pressure. For each variable, measures are acquired hourly.

For our needs, we used only the mean 10 m wind speed and direction, the mean global radiation, the mean atmospheric pressure, the precipitation, the 2 m relative humidity, and the surface temperature. The objective of the present study is to develop and identify a procedure that optimizes hydrodynamic modeling output. With this intent, we used the WRF simulations (values varying in time and space) as a forcer in the Mike model, and we compared the results with the Mike forced with constant values (constant in time and space) and values measured by the weather station (domain-constant and time-varying).

The purpose, then, is to replace domain-constant and time-varying weather data with both time- and domain-varying weather data. With the WRF model, 4D analysis of meteorological fields over the Taranto area with surface spatial resolution of 1 km and temporal resolution of 1 h were derived. The WRF output variables to be entered as input into the Mike model include: U10 (x-axis component of wind speed vector), V10 (y-axis component of wind speed vector), PSFC (atmospheric pressure), T2 (air temperature), SST (temp.superf.water), RH2 (relative humidity), RadSol (solar rad.), PREC (precipitation). Pairing the two models, WRF and Mike, involves difficulties caused by the difference in data format: the output data of the WRF model are in NetCDF (Network Common Data Form) format, while the Mike model requires as input data dfs2 format. Hence, it was necessary to proceed with the implementation of a dedicated Matlab script developed to prompt the WRF output variables and process them to obtain Mike's useful parameters. Not all WRF variables are used in the Mike model. However, it is possible to use the available variables and process them to estimate additional variables. Afterward, the input data to Mike in the dfs2 format should be derived.

2.3.4. Application of Procedure to the Case Study

After the WRF model integration procedure in the Mike model, we analyzed a case study concerning the Mar Piccolo and Mar Grande basins. The parameters used to run the WRF model are listed below:

- WRF input: Analysis-ECMWF 0.16° (spatial resolution about 16 km and temporal resolution of 6 h);
- Output temporal resolution: 1 h—Spatial resolution output: 1 Km—Scaling: 4–1;
- Run period: 7 July 2019–19 February 2019.

Three hydrodynamic simulations were conducted:

1. Hydrodynamic simulation without meteorological forcing (constant in time and space);
2. Hydrodynamic simulation with meteorological forcing from ARPA Puglia ground station (time-varying but constant forcing in space);
3. Hydrodynamic simulation with forcing from WRF model output (varying in both time and domain).

For each simulation, 2 cases related to strong wind from NNW and weak wind from ESE were compared, respectively. The present study was conducted with reference to the year 2019. The choice to refer the study to the year 2019 is mainly due to the availability of data. The year 2019 represents the one in which more data and field surveys were available as well as data on the Copernicus Emodnet portals.

2.4. Comparison with Measured Values

For the comparison between simulations and field measurements, we referred to studies published previously in the relevant literature. In particular, in Armenio et al. [1,2,4], data measured by fixed oceanographic stations located in the Mar Grande and Mar Piccolo basins were compared with the current's values obtained from the model. Although these studies refer to previous years, it must be considered that the setup of the MIKE model adopted for our goal is unchanged except for the meteorological forcing. In any case, in the present case study, we also compared the currents derived from the model and field measurements carried out during the same period (January–February 2019) in the Mar

Grande area. These concern surface sea current measurements carried out by ARPA Puglia with a propeller water current meter as part of the monitoring of marine coastal waters in the Apulia Region. The position of the sampling points where the probe was placed is shown in Figure 1d. Field measurements refer to surface currents over a few hours. For comparison with the current data, the average value of current speed and directions during the measurement time were considered.

Figure 3 shows the stick plots of the current velocities extracted from numerical modeling WRF forcing at the sampling stations identified in Figure 2d. Vectors marked in red represent field measurements.
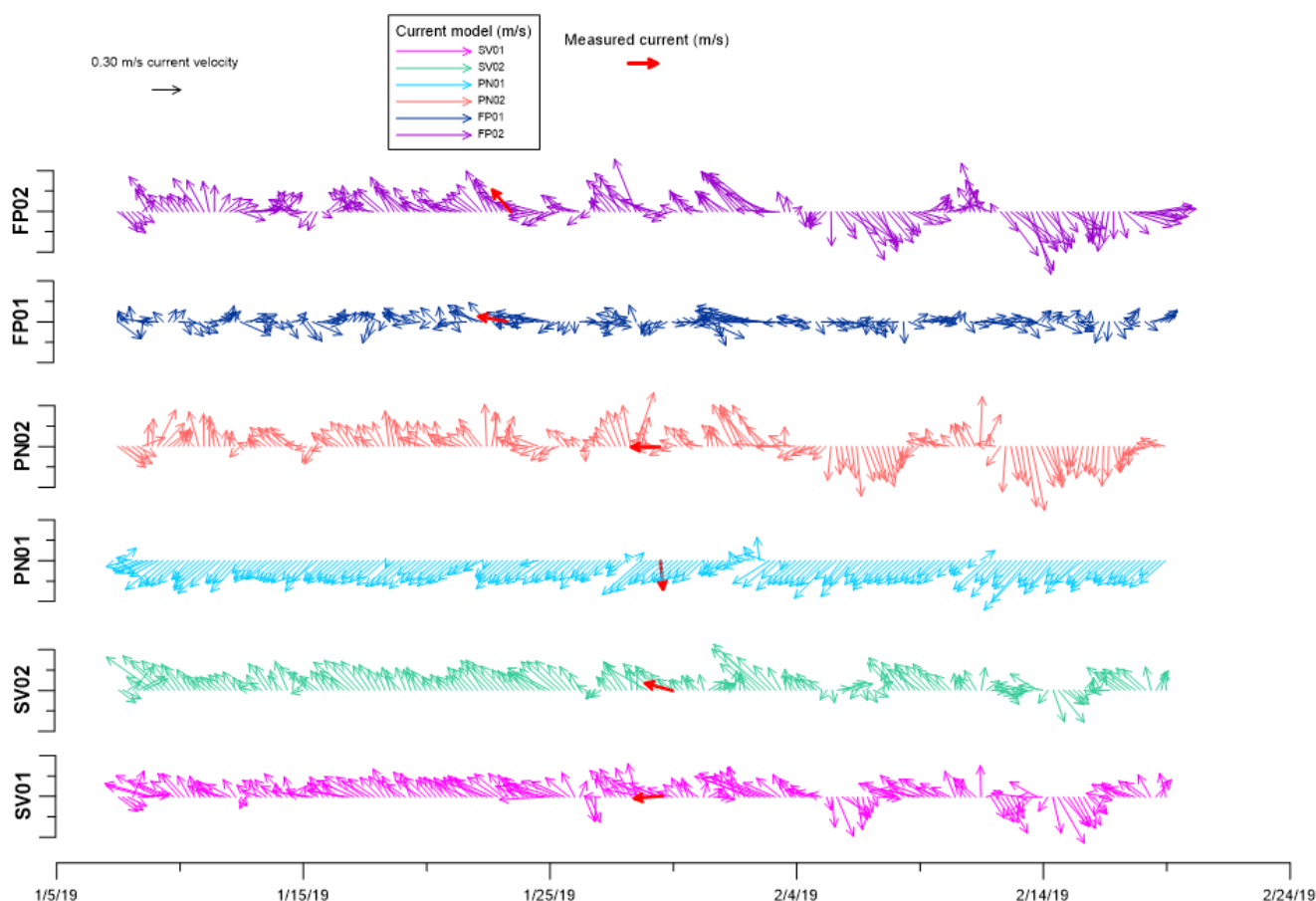

Figure 3. Stick plot of modeled current extracted from numerical modeling WRF forcing. (Source: authors' elaboration).

Comparison with the measured values of the velocities measured at the field stations showed the same orders of magnitude in terms of current intensity. In addition, a comparison was carried out with the current velocity measurements extracted from the oceanographic buoy located in the Mar Grande basin for the same reference period (January–February 2019); again, comparable values of current intensities were found. More details on the description of the buoy in the Mar Grande basin can be found in [3,4].

3. Results

3.1. Comparison of the Results

The results obtained for the two situations occurring in the study area are reported: the first case related to the day 13 February 2022 at 02:00 p.m., in which a strong wind occurred and the second case of the day 18 February 2022 at 04:00 a.m. in which a weak wind was detected.

3.1.1. Case Study of Intense Wind Speed Coming from NNW

This case study is on 13 February 2019 at 02:00 p.m. At this time, the ground station located in S. Vito has measured a wind speed of 14.1 m/s coming from NNW (353°).

Figure 4 shows graphically an output sub-set of the hydrodynamic simulation obtained for the Mar Piccolo and Mar Grande basins, respectively, for the three scenarios investigated. In particular, Panels (a), (b) and (c) represent the current outputs obtained, respectively, with meteorological forcing from WRF (varying in both time and space), from the ARPA ground station (space constant and time variable) and no wind forcing (constant in both time and space) in Mar Piccolo, and Panels (d), (e) and (f) reproduce the same scenarios for the Mar Grande area, respectively. The maps shown in Figure 4 represent the pattern of surface circulation currents; the color scale is representative of current intensity (velocity), and the vectors indicate the direction of current flow. The violet vectors were added manually to remark the prevailing directions of the main current flow. Looking at Figure 4a, WRF forcing, it should be noted that there are areas (red colored) where the currents are more intense (above 0.22 m/s); in particular, along the eastern shore of the I and II Bays of Mar Piccolo. The prevailing current directions are north-northwest, consistent with the direction from which the wind blows. The same considerations apply to the Mar Grande basin, Figure 4d, where higher average intensity values are observed than in the Mar Piccolo basin. In Panels (b) and (e) (meteorological forcings varying only in time but constant in space), it is observed that the current flows show the same prevailing directions as in Panels (a) and (d) but with slightly lower intensity values. We can see a very different situation in Panels (c) and (f), simulation without meteorological forcing. Sea current velocity varies in the range of 3 cm/s–7 cm/s, whereas the current directions are significantly different from the two previous scenarios for both the Mar Piccolo and Mar Grande basins. It is worth noting that in this latter simulation, since the effect of wind forcing was not computed, the current directions are the result of the other forcings acting on the site. By comparing Figure 4a–d with Figure 4b–e, since strong winds from the NNW were considered in both simulations, the differences obtained can be attributed to a sensitivity of the sea currents not only to the wind intensity but also to its spatial gradient (in Section 3.2 we report a detailed description).

3.1.2. Case Study with Weak Wind Coming from the ESE

This case study is on 18 February 2019 at 04:00 a.m. At this time, the ground station located in S. Vito has measured a wind speed of 1.4 m/s coming from the SSE (116°).

Figure 5 shows graphically an output sub-set of the hydrodynamic simulation obtained for the Mar Piccolo and Mar Grande basins, respectively, for the three scenarios investigated. In particular, Panels (a)–(c) represent the current outputs obtained respectively with meteorological forcing from WRF (varying in both time and space), from the ARPA ground station (space constant and time variable) and no wind forcing (constant in both time and space) in Mar Piccolo, and Panels (d), (e) and (f) reproduce the same scenarios for the Mar Grande area, respectively. It can be observed that also in the case of a weak wind speed, the current directions obtained without computing the meteorological forcing, Panels (c)–(f) are completely different from the other simulations investigated, i.e., meteorological forcing from the WRF model, Panels (a)–(d) and meteorological forcing with ground station, Panels (c)–(f). Comparing the outcome of Panels (a)–(d) with (c)–(f), it should be noted that they show similar current directions, but the current velocity is slightly higher for the WRF meteorological scenario.
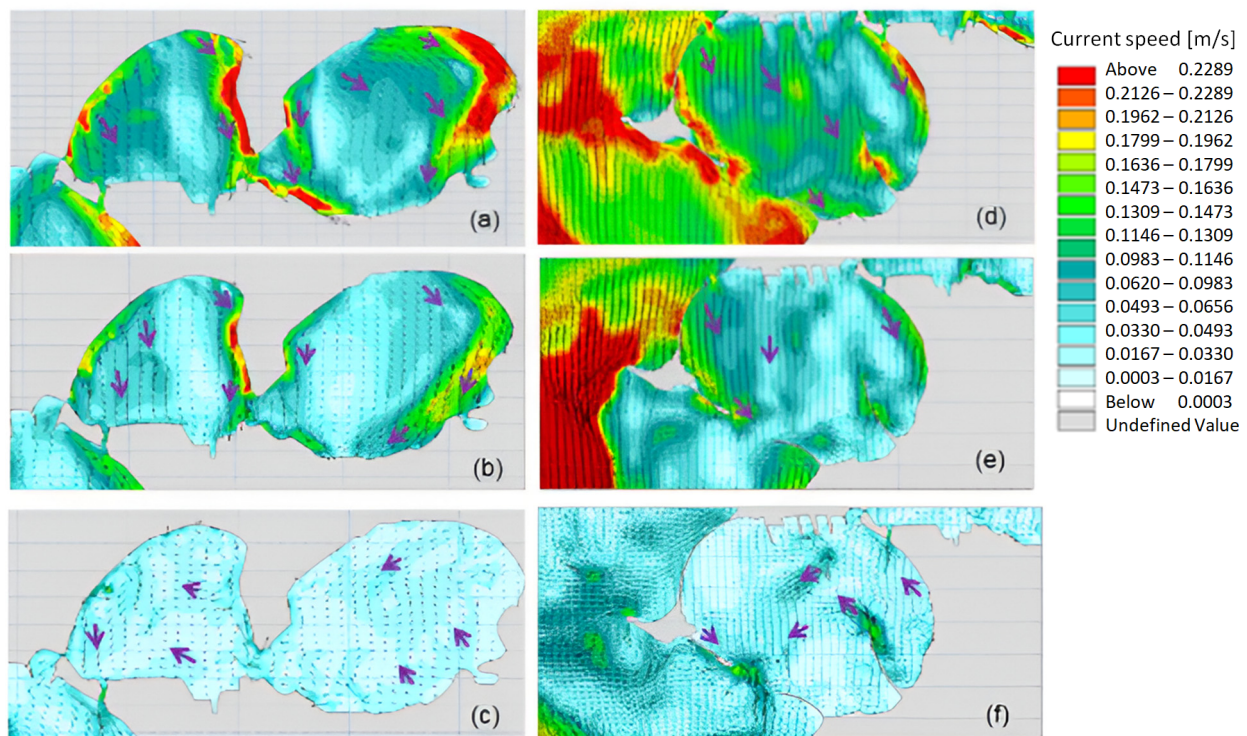
Figure 4. Model current results for the case of intense wind coming from the NNW: (**a**) meteorological forcing from WRF, (**b**) meteorological forcing from the ARPA ground station (space constant and time variable) and (**c**) no wind forcing in Mar Piccolo. (**d**–**f**) reproduce the same scenarios for the Mar Grande basin, respectively. The violet vectors were added manually. (Source: authors' elaboration).
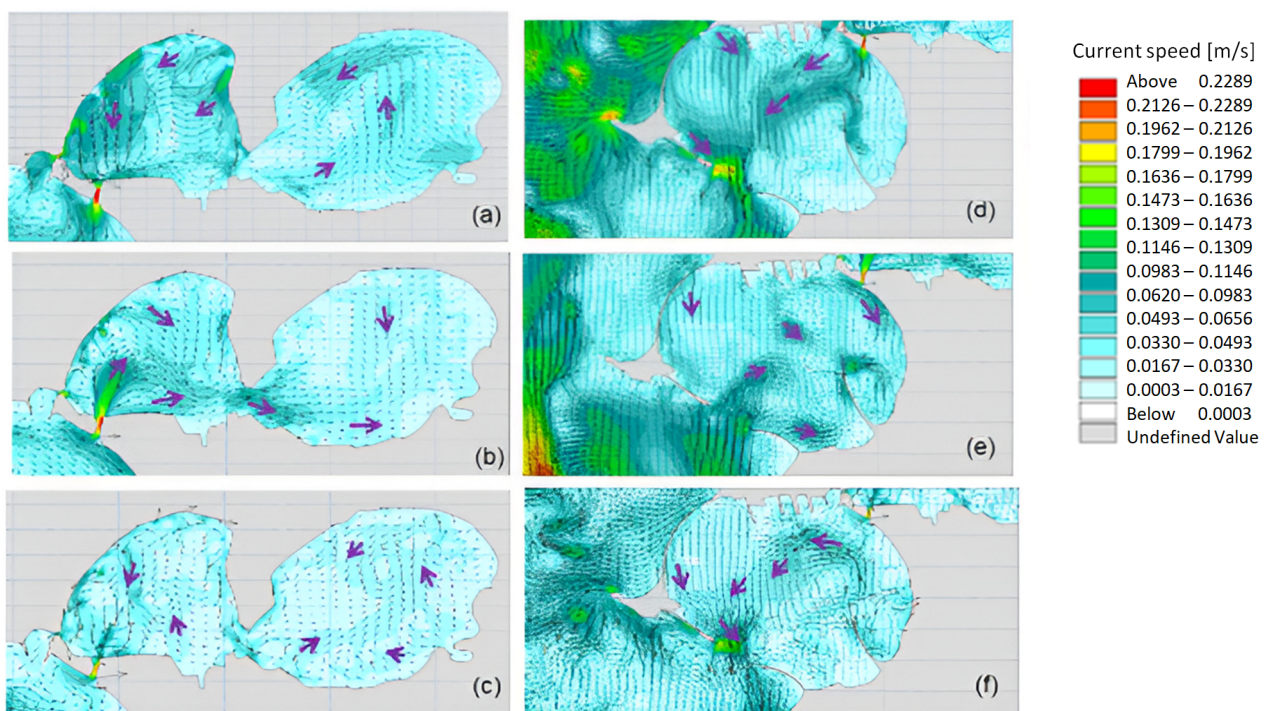

Figure 5. Model current results for the case of weak wind coming from the SSE: (**a**) meteorological forcing from WRF, (**b**) meteorological forcing from the ARPA ground station (space constant and time variable) and (**c**) no wind forcing in Mar Piccolo. (**d**–**f**) reproduce the same scenarios for the Mar Grande basin, respectively. The violet vectors were added manually (Source: authors' elaboration).

3.2. Analysis of the WRF Model Output

Analyzing the meteorological data both measured and simulated, it is possible to conclude that wind is not uniform and constant in modulus and direction over the whole area of interest. In fact, by comparing the values measured by two ground stations located in the same area of interest, it can be observed that the wind is not constant over the whole area. Specifically, as shown in Figure 6, the two ground stations, one located in San Vito and the other in the ENI plant in Taranto, about 10 km apart, measure a wind speed that differs by about 5 m/s. Therefore, using only the data measured by one of the ground stations for the whole area is certainly unrealistic as it is also evident from the output values in the WRF model under analysis.
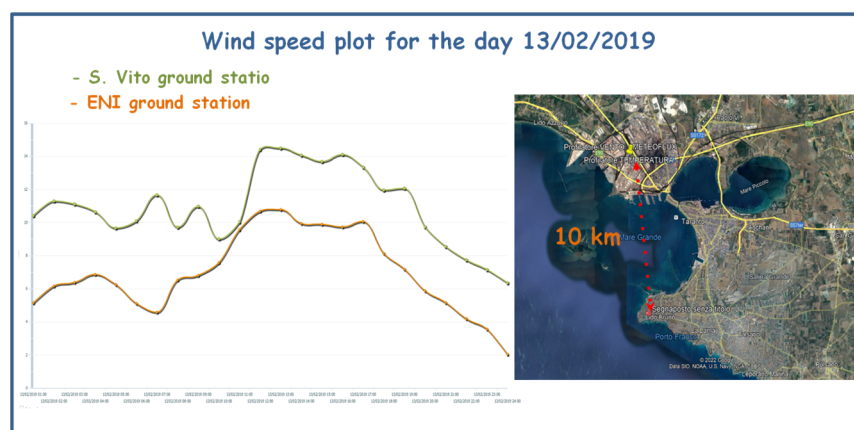

Figure 6. Comparison between the wind speed measured by the station located in San Vito (south) and the ground station located in ENI plat (north) in Taranto for the day 13 February 2019. (Source: authors' elaboration).

In Figure 7, we show the distribution of wind speed simulated with the WRF model on the area of interest for the day 13 February 2019 during hour 02:00 p.m., which was characterized by synoptic situations of intense wind speed with uniform wind direction pattern. The histogram refers to all values estimated by the WRF model for each point in the output domain at 1 km spatial resolution. The histogram shows that wind speed takes different values at different points in the area of interest. Measured and simulated data at San Vito station show a deviation of about 3 m/s. It should be noted that the WRF output concerns points in a regular grid with 1 km resolution, and it is not certain that the coordinates of interest fall in one of the grid points. For this reason, specific software is used, such as GrADS (Grid Analysis and Display System), which provides the desired value through complex interpolations from the values in the grid points. Another way to estimate the specific point simulated value is to consider the average value obtained from the WRF model at four grid points around the point of interest. In the present analysis, this averaging methodology led to a reduction in the difference between measured and simulated wind speed data from 3 m/s to 1 m/s. We also considered a weak wind speed case. In Figure 8, the WRF simulated wind speed is shown for 9 February 2019 at 05:00 p.m. in the area of interest. The image was created with the GrADS software, and therefore, the coasts represented are a modeling approximation of the real situation. It is characterized by low-intensity values and a uniform wind direction pattern. As shown, wind cannot be considered as a constant over an extended area, thus considering just one measured wind value to represent an entire area may lead to an unrealistic meteorological description. The WRF model result is useful to provide reliable point wind data over the area of interest, also where no ground station is available, allowing a better and more realistic meteorological description.
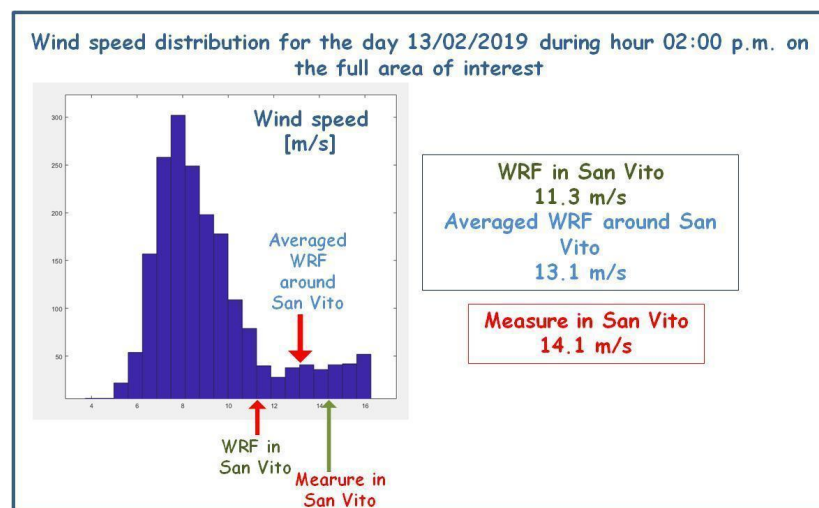
Figure 7. Histogram of wind speed simulated with the WRF model on the area of interest for the day 13 February 2019 during hour 02:00 p.m. Both values simulated and measured in the coordinate of the San Vito ground station are reported. In addition, the value obtained by averaging the simulated values around the coordinates of the San Vito ground station is also reported. (Source: authors' own elaboration).
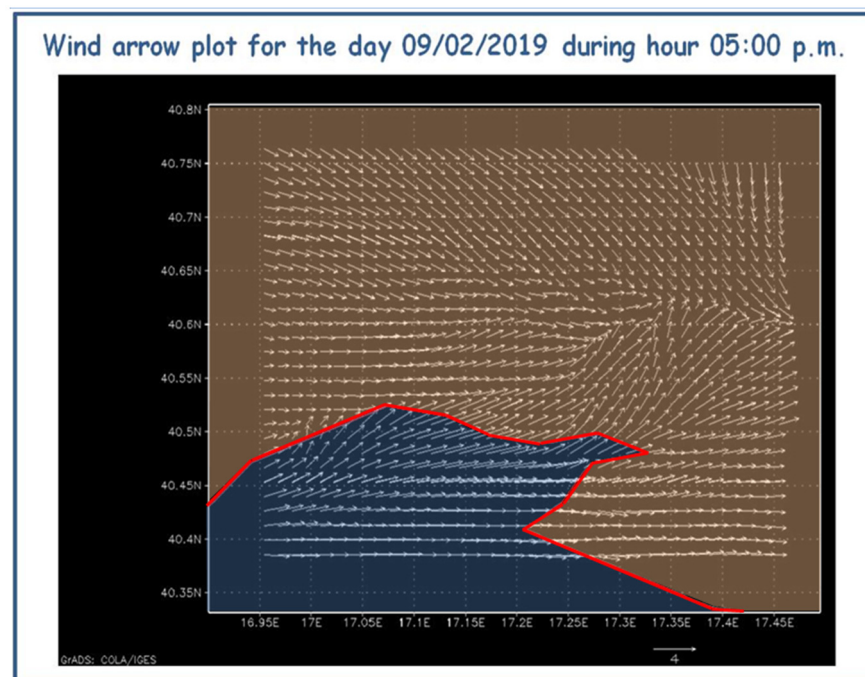

Figure 8. Wind arrow plot simulated for the day 9 February 2019 during hour 05:00 p.m. on the full area of interest. Red line: coast used for modeling. (Source: authors' elaboration).

3.3. Analysis of Wind-Induced Current Variability

To investigate the variability of currents with respect to the meteorological forcing, Figure 9 displays for the Mar Piccolo basin the vectors of modeled sea current velocity with reference to the case of intense wind from the NNW that occurred on 13th February 2019 at 02.00 p.m. The vectors were extracted at selected points marked T1 to T10 and representing the sea current velocities and directions respectively corresponding to the three scenarios analyzed, i.e.:

1. Sea currents resulting from the hydrodynamic simulation performed with meteorological forcing from the WRF model (red vector);
2. Sea currents resulting from the hydrodynamic simulation performed with meteorological forcing from the ARPA ground station, variable in time but constant in space (green vector);
3. Sea currents resulting from the hydrodynamic simulation performed with no meteorological forcing computed (blue vector).
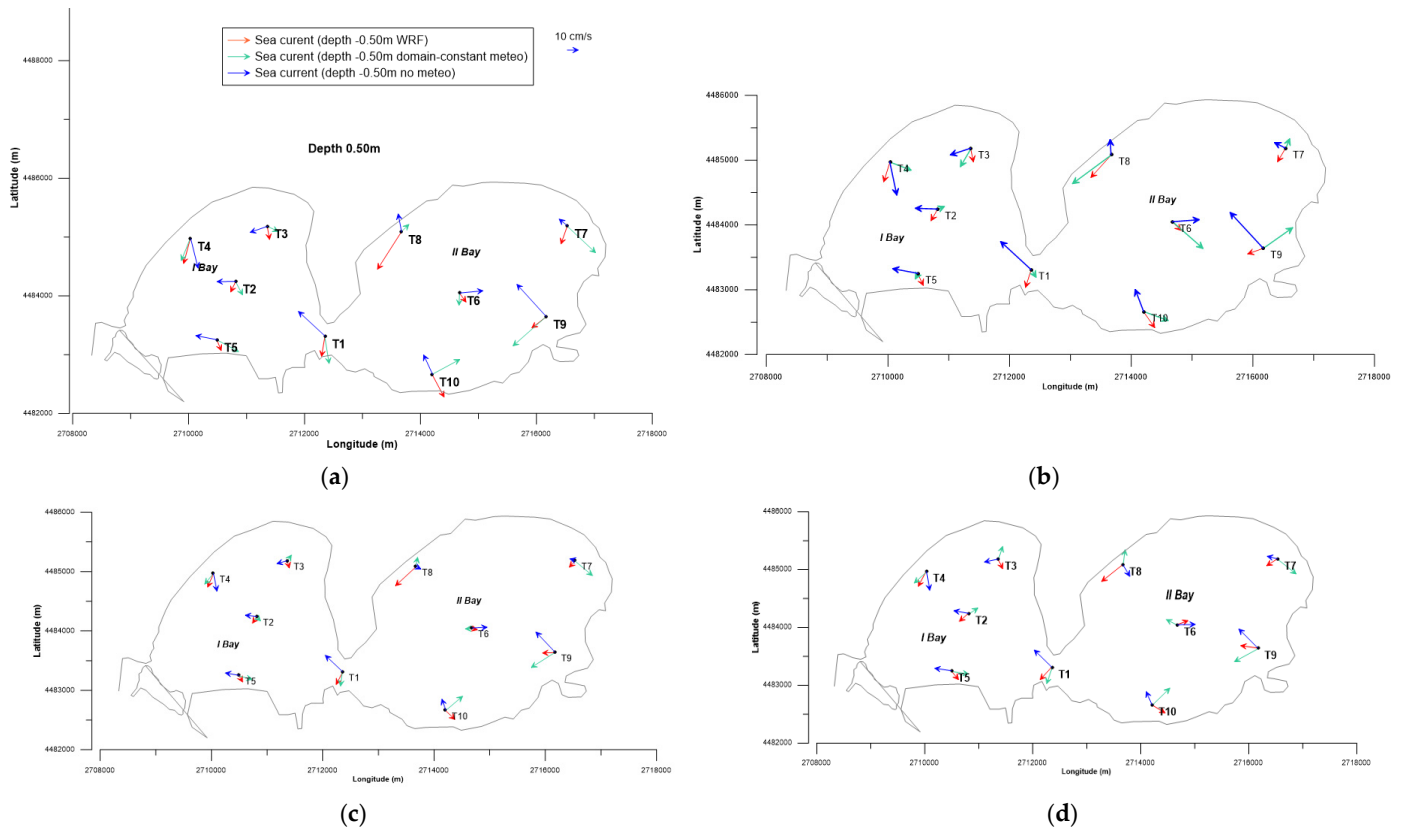

(a)

(b)

(c)

(d)

Figure 9. Modeled sea current obtained in Mar Piccolo by using (red) meteorological forcing from the WRF model; (green) domain-constant data and (blue) no meteorological forcing. Vector data refer to (**a**) 0.5 m, (**b**) 1.0 m, (**c**) 1.5 m and (**d**) 2.0 m water depth from the surface. (Source: authors' elaboration).

The extracted data refer to the case of intense wind from the NNW that occurred on 13 February 2019 at 02.00 p.m. In Figure 9, vectors were reported for water depths of (a) 0.5 m, (b) 1.0 m, (c) 1.5 m and (c) 2.0 m. Hereafter, for the sake of simplicity, we refer to blue, green and red vectors to respectively recall the numerical simulations mentioned above. From Figure 9, it can be seen that the blue vectors generally show higher intensities than those representing the other two scenarios analyzed. It is particularly evident in transects T1, T5 and T9. Such a discrepancy is more noticeable for sea currents at the surface (Figure 9a,b) and less so at deeper depths (Figure 9c,d). Concerning the wind direction (NNW), it is worth considering that transects T5 and T9 are located in the I and II Bays of the Mar Piccolo basin in the SSE position, respectively. In the actual case, it comes into consideration that the wind blows through the entire surface of the I and II sinus before reaching the positions where transects T5 and T9 are located. Along its path, the wind blowing influences the water masses' movement on the surface. On the contrary, in the case of the simulation without wind forcing (blue vectors), the wind-blowing action on the surface water is not taken into the computation. Hence the water mass movement is imputable to other forcings. It is also noted that this wind-blowing effect is more noticeable at the water surface than the currents measured at deeper water depths.

In particular, transect T1 is located at the midpoint between the I and II Bays where there is a constriction of the basin's cross section due to its morphology. Even for this transect, although morphological constraints limit the water flow considerably, a change in the direction of the sea currents with respect to the type of meteorological forcing can be noted. Specifically, at T1, the red and green vectors exhibit similar intensities, though the directions are slightly different. The red vectors (WRF) tend to rotate towards the SSW. Regarding the transect at point T4 located not far from the coastline, it is observed that the red vectors remain constant in direction and intensity for the various depths while the green ones denote an appreciable variability of directions. The blue vectors present constant directions and intensities directed towards S. The T3 vector is located north of I Bay. The current intensities detected over there are lower than the intensities computed in the other transects of I Bay. Also in this case, it can be noticed that although the blue and red vectors hold almost constant directions at the examined water depths, on the contrary, the green vectors reveal greater variability: at depths of 0.5 m, they proceed towards the E; at depths of 1.0 m, they proceed towards the SSW; at depths of 1.5 m and 2.0 m, they proceed towards the NNE. A similar pattern can be detected in transect T8: the red vectors show a constant, SW-directed direction for the various depths. In opposite, the blue vectors are directed towards the N for depths of 0.5 m and 1.0 m, while deeper (1.5 m and 2.0 m) they rotate towards the E. The red vectors keep a constant direction parallel to the coast for the varying depths. In Transect T6, the red vectors are pointing E at all the depths investigated. Conversely, the green vectors show more variability. In transects T7 and T9, it is observed that the blue vectors feature the same direction, which is also constant with depths and directed towards the NW with higher intensities in T9. The red vectors of T9 are directed toward W. It is worth noting that the transect is in the proximity of the D'Ajedda channel and the sea currents suffer from this contribution. Green vectors again feature higher variability and even opposite directions with depths (see 0.5 m and 1.0 m). In transect T10, the greens and reds have similar current intensities. The greens detect more directional variability with water depth than the reds, which continue in an almost constant, SSE-directed direction. Figure 10 reports for the Mar Grande basin, for the points marked T1 to T5, the vectors representing the velocities and directions of the currents corresponding, respectively, to the three scenarios already described for the Mar Piccolo case. As in the case of the Mar Piccolo, current values were extracted at depths of (a) 0.5 m, (b) 1.0 m, (c) 1.5 m and (d) 2.0 m. Generally, the current directions are more consistent than the prevailing wind direction (intense wind from the NNW). At point T1, it is noticeable that the current vectors are directed for all the depths analyzed towards S. The highest intensities are found for the red vector and the lowest for the blue vector (without meteorological). In addition, the red vector has the greatest direction deviation with depth. Point T2 is located in the center of the Mar Grande basin. At this point, the blue vectors are constant in intensity and direction and directed toward the SSW. The green and red vectors hold constant directions in the investigated depths and slightly increase in intensity at depths of 1.5 m and 2.0 m. Point T3 exhibits consistent directions toward the ESE. Points T4 and T5 are the points where the lowest current intensities are detected. In these areas, currents are affected by the coastline and jetties that constrain the direction of current flow. Generally, the reproduced velocity values are in the range [0.02 m/s–0.1 m/s] with some peaks (0.2 m/s) along the Navigable Channel. The lowest current velocity values occur in the II Bay. Figure 11 illustrates boxplots of the current velocities measured for the three scenarios examined. Figure 11a–c refer to the Mar Grande basin and Figure 11d–f for the Mar Piccolo basin, respectively. It may be observed that the boxplot (a) relating to the simulation executed with punctual meteorological forcing reveals a greater dispersion of the sea current velocity variable especially for transects T6 and T8. Boxplot (b) (WRF meteorological) exhibits less current variability, also for transect T8. On the contrary, in boxplot (c), the dispersion of the current variable is minimal, especially in transects T2, T3, T5 and T6. Generally, boxplots of Mar Piccolo show a left asymmetry

(more pronounced lower whisker) of the data. Specifically, a current data tendency to disperse towards smaller values than the middle one is observed. As regards the Mar Grande basin, it can be observed that boxplot (c) also exhibits the lowest dispersion of the current variable. Whereas boxplot (a) is the one showing the highest dispersion as well as tendentially higher current values than in the case of boxplot (b). Looking at the boxplot of Mar Grande, it can be noticed that the left asymmetry observed in the Mar Piccolo basin is not present, and the data tend to be more uniformly distributed.

(**a**)

(**b**)

(**c**)

(**d**)

Figure 10. Modeled sea current obtained in Mar Grande by using (red) meteorological forcing from the WRF model; (green) domain-constant data and (blue) no meteorological forcing. Vector data refer to (**a**) 0.5 m, (**b**) 1.0 m, (**c**) 1.5 m and (**d**) 2.0 m water depth from the surface. (Source: authors' elaboration).
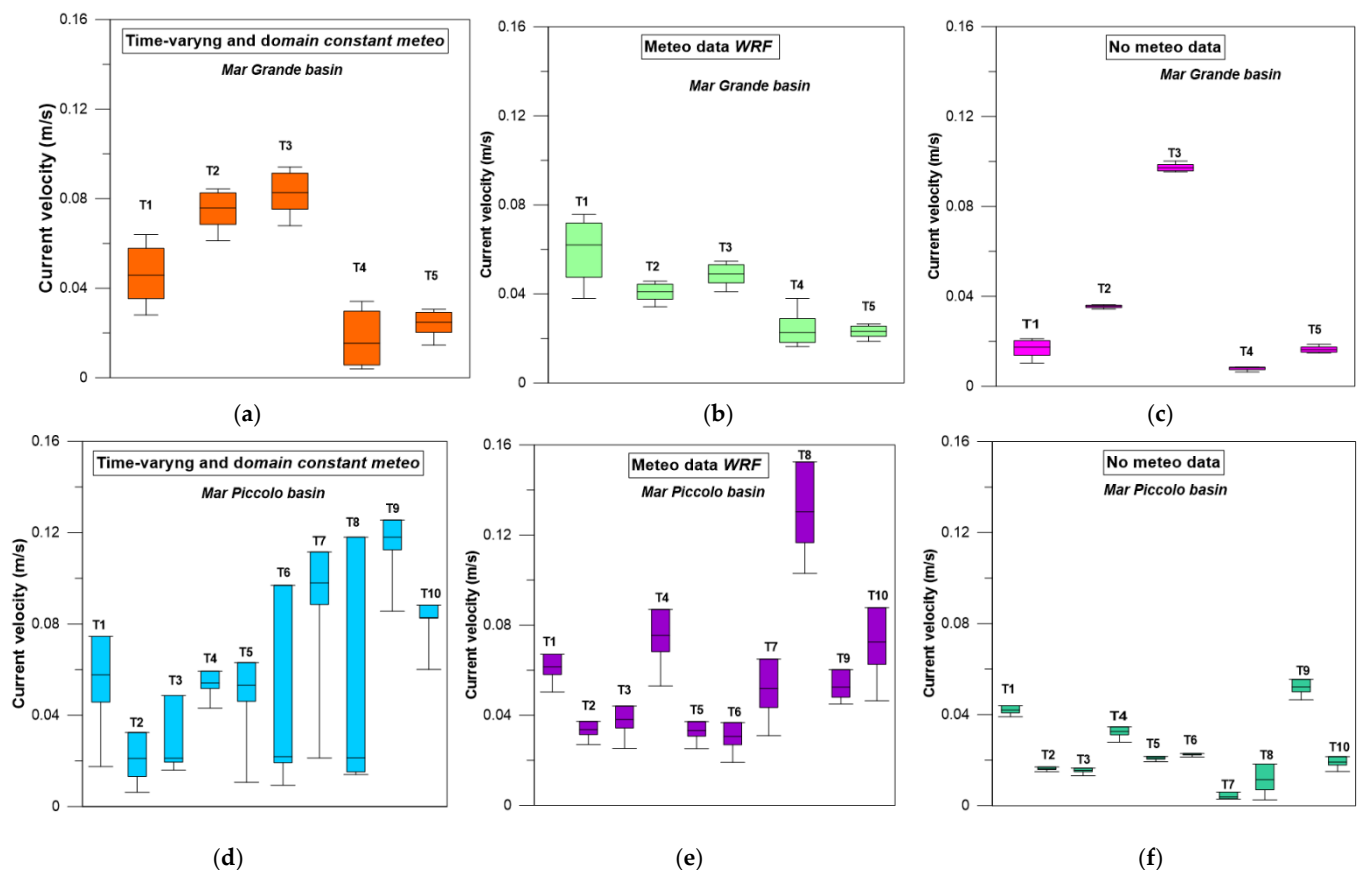
Figure 11. Boxplots of model current results for the case of intense wind. Mar Grande (**a**) meteorological forcing from the WRF model; (**b**) meteorological forcing from the ARPA station (space constant and time variable) and (**c**) no wind forcing. Figure (**d–f**) reproduce the same scenarios for the Mar Piccolo basin, respectively. (Source: authors' elaboration).

4. Discussion

From the investigations conducted in the transects shown in Figures 9–11, the blue vectors (no meteorological forces) have almost constant directions in the depths analyzed. Their intensities are higher than in simulations in which the meteorological conditions are computed. In the Mar Piccolo basin, can be observed that the currents in this case (no meteorological scenario) have prevailing directions towards the NNE and hence in the opposite of the wind (the wind blows from the NNW).

The current, therefore, without wind would proceed in the opposite direction. This proves the effect of the wind in such basins: the wind influences surface currents, driving them sometimes in the opposite direction to the one they would have without wind. In such a case, the wind acts by varying not only the directions but also by damping the intensities. Although wind-induced currents may be important, other causes are certainly responsible for the currents in the absence of wind. One of these is the tide, whose effect is most strongly noticeable in semi-enclosed basins such as the Mar Piccolo. Exactly on 13 February at 02:00 p.m., there was low tide, while on 18 February at 04:00 a.m., there was peak high tide. If we look at the cases of the simulations in which the wind forcing was computed both as a point input varying only in time and as an input varying both in time and in space (WRF), we observe that the intensities of the currents in the various transects are generally lower than those computed in the absence of wind forcing. A comparison of the results obtained for these simulations, i.e., spatial constant meteorological (green vectors) and WRF meteorological (red vectors), also reveals that: the red vectors maintain constant directions along the analyzed depths, and intensities tend to decrease for increasing depths. Conversely, the green vectors show higher variability compared to water depth with respect

to both directions and intensities. The case study highlighted that for a semi-enclosed coastal basin such as Mar Piccolo, using a space-constant and time-varying meteorological forcing has resulted in currents with higher spatial variability in terms of both direction and intensity. The use of a WRF model meteorological forcing (variable both in time and domain) revealed less variability in current intensities and directions. The higher stability of currents observed with the WRF simulation does not mean that the wind forcing is less significant in this case. Rather, it is worth considering that the representative vectors of the sea currents are the result of various forcing factors (discharges, drains, citres, inputs) affecting the basin, including the meteorological forcing, and the currents are also constrained by the peculiar morphology of the basin itself, which hinders their movement. Referring to the red and green vectors, it is observable in general that the hydrodynamic simulations with the WRF meteorological model reveal more intense sea currents only at points T1, T8 and T10. Whereas for the other points, the current intensities are roughly similar. Concerning the direction deviation between the green and red vectors, it is noted that the maximum discrepancy is of the order of 20°. When comparing the blue vectors (without meteorological forcing) with the red and green ones, it can also be noted that the blues have different directions and intensities at the various points analyzed. Even in the case of the Mar Grande basin, the effect of the wind forcing on the marine circulation and the importance of its computation is evident. Nevertheless, the difference between the spatial constant meteorological forcing and that from the WRF model is less appreciable. For the case of the Mar Grande basin, a more consistent trend of the extracted currents is noted for the three analyzed scenarios. This may be imputable to several factors, e.g., it is a larger basin with a circular shape and greater water depth. In addition, there are fewer citri, so the thermohaline action generated by them is less influential.

5. Conclusions

A coupled meteo–hydrodynamic approach consisting of the WRF meteorological model and Mike (DHI) hydrodynamic model was executed in semi-enclosed basins to investigate the sensitivity of the sea current pattern as a function of the type of meteorological forcing. The methodological approach used involved the implementation of a specific operational procedure for interfacing the WRF model and the Mike circulation model. Three different modeling scenarios were set up by varying the meteorological forcing. Run tests of the hydrodynamic model were conducted by using meteorological forcing of the data acquired by the closest ground station (time-varying data but constant in the domain). In addition, run tests of the coupled meteo–hydro model were also performed by using the meteorological forcing of the output file processed by the WRF model (domain- and time-varying data). The no meteorological forcing scenarios were also executed to appreciate the contribution of meteorological drive current. The results obtained for the two situations occurring in the study area are reported: the first case related to the day 13 February 2019 at 02:00 p.m., in which a strong wind occurred, and the second case of the day 18 February 2019 at 04:00 a.m., in which a weak wind was detected. To investigate the variability of currents with respect to the meteorological forcing, modeled sea current data were compared for the three scenarios analyzed.

The results obtained with this approach provide significant insight into the meteo–hydrodynamic modeling of semi-enclosed basins showing a different variability of meteo-driven current for the cases analyzed. The effect of the wind in such basins is relevant, and the two semi-enclosed basins, despite the same scenarios, showed different effects on the circulation current. Finally, we consider that, even though about five years have passed, the parameters analyzed in the present study have not changed significantly as they are representative of typical trends at the study site, as shown in previous studies.

References

1. Armenio, E.; Meftah, M.B.; Bruno, M.F.; De Padova, D.; De Pascalis, F.; De Serio, F.; Di Bernardino, A.; Mossa, M.; Leuzzi, G.; Monti, P. Semi enclosed basin monitoring and analysis of meteo, wave, tide and current data: Sea monitoring. In Proceedings of the 2016 IEEE Workshop on Environmental, Energy, and Structural Monitoring Systems (EESMS), Bari, Italy, 13–14 June 2016; pp. 1–6.
2. Armenio, E.; De Serio, F.; Mossa, M. Analysis of data characterizing tide and current fluxes in coastal basins. *Hydrol. Earth Syst. Sci.* **2017**, *21*, 3441–3454.
3. De Serio, F.; Malcangio, D.; Mossa, M. Circulation in a Southern Italy coastal basin: Modelling and field measurements. *Cont. Shelf Res.* **2007**, *27*, 779–797. [CrossRef]
4. Armenio, E.; De Padova, D.; De Serio, F.; Mossa, M. Monitoring system for the sea: Analysis of meteo, wave and current data. In Proceedings of the IMEKO TC19 Workshop on Metrology for the Sea MetroSea, Naples, Italy, 11–13 October 2017; pp. 143–148.
5. Roland, A.; Cucco, A.; Ferrarin, C.; Hsu, T.-W.; Liau, J.-M.; Ou, S.-H.; Umgiesser, G.; Zanke, U. On the development and verification of a 2-D coupled wave-current model on unstructured meshes. *J. Mar. Syst.* **2009**, *78*, S244–S254. [CrossRef]
6. Pascalis, F.D.; Petrizzo, A.; Ghezzo, M.; Lorenzetti, G.; Manfè, G.; Alabiso, G.; Zaggia, L. Estuarine circulation in the Taranto Seas. *Environ. Sci. Pollut. Res.* **2016**, *23*, 12515–12534. [CrossRef]
7. Gaeta, M.G.; Samaras, A.G.; Federico, I.; Archetti, R.; Maicu, F.; Lorenzetti, G. A coupled wave–3-D hydrodynamics model of the Taranto Sea (Italy): A multiple-nesting approach. *Nat. Hazards Earth Syst. Sci.* **2016**, *16*, 2071–2083. [CrossRef]
8. Ferrarin, C.; Davolio, S.; Bellafiore, D.; Ghezzo, M.; Maicu, F.; Mc Kiver, W.; Drofa, O.; Umgiesser, G.; Bajo, M.; De Pascalis, F.; et al. Cross-scale operational oceanography in the Adriatic Sea. *J. Oper. Oceanogr.* **2019**, *12*, 86–103. [CrossRef]
9. Zarzuelo, C.; López-Ruiz, A.; Bermúdez, M.; Ortega-Sánchez, M. Measurements and modeling of water levels, currents, density, and wave climate on a semi-enclosed tidal bay, Cádiz (southwest Spain). *Earth Syst. Sci. Data* **2023**, *15*, 3095–3110. [CrossRef]
10. Monti, P.; Leuzzi, G. Lagrangian models of dispersion in marine environment. *Environ. Fluid. Mech.* **2010**, *10*, 637–656. [CrossRef]
11. Scroccaro, I.; Matarrese, R.; Umgiesser, G. Application of a finite element model to the Taranto Sea. *J. Chem. Ecol.* **2014**, *20* (Suppl. S1), 205–224. [CrossRef]
12. Mike 21 & Mike 3 Flow Model FM 2021. DHI A/S Headquarters. Available online: https://www.mikepoweredbydhi.com/download/product-documentation (accessed on 30 January 2022).
13. Skamarock, W.C.; Klemp, J.B.; Dudhia, J.; Gill, D.O.; Liu, Z.; Berner, J.; Wang, W.; Powers, J.G.; Duda, M.G.; Barker, D.M.; et al. 2019: A Description of the Advanced Research WRF Version 4. Available online: https://opensky.ucar.edu/islandora/object/technotes:588 (accessed on 30 January 2022).
14. Alabiso, G.; Giacomini, M.; Milillo, M.; Ricci, P. The Taranto sea system: 8 years of chemical–physical measurements. *Biol. Mar. Medit.* **2005**, *12*, 369–373.
15. Parenzan, P. Il Mar Piccolo e il Mar Grande di Taranto. *Thalass. Salentina* **1969**, *3*, 19–36.
16. Buccolieri, A.; Buccolieri, G.; Cardellicchio, N.; Dell'Atti, A.; Di Leo, A.; Maci, A. Heavy metals in marine sediments of Taranto Gulf (Ionian Sea, southern Italy). *Mar. Chem.* **2006**, *99*, 227–235. [CrossRef]
17. Di Leo, A.; Annicchiarico, C.; Cardellicchio, N.; Spada, L.; Giandomenico, S. Trace metal distributions in Posidonia oceanica and sediments from Taranto Gulf (Ionian Sea, Southern Italy). *Mediterr. Mar. Sci.* **2013**, *14*, 204–213. [CrossRef]
18. Cardellicchio, N.; Annicchiarico, C.; Di Leo, A.; Giandomenico, S.; Spada, L. The Mar Piccolo of Taranto: An interesting marine ecosystem for the environmental problems studies. *Environ. Sci. Pollut. Res.* **2016**, *23*, 12495–12501. [CrossRef]
19. Braga, F.; Ciani, D.; Colella, S.; Organelli, E.; Pitarch, J.; Brando, V.E.; Bresciani, M.; Concha, J.A.; Giardino, C.; Scarpa, G.M.; et al. COVID-19 lockdown effects on a coastal marine environment: Disentangling perception versus reality. *Sci. Total Environ.* **2022**, *817*, 153002. [CrossRef]

20. Moharir, R.V.; Khairnar, K.; Paunikar, W.N. MIKE 3 as a modeling tool for flow characterization: A review of applications on water bodies. *Int. J. Adv. Stud. Comput. Sci. Eng.* **2014**, *3*, 32.

21. Trotta, F.; Pinardi, N.; Fenu, E.; Grandi, A.; Lyubartsev, V. Multinest high resolution model of submesoscale circulation features in the Gulf of Taranto. *Ocean Dynam.* **2017**, *67*, 1609–1625. [CrossRef]

22. Mondal, K.; Bandyopadhyay, S.; Karmakar, S. Framework for global sensitivity analysis in a complex 1D-2D coupled hydrodynamic model: Highlighting its importance on flood management over large data-scarce regions. *J. Environ. Manag.* **2023**, *332*, 117312. [CrossRef]

23. Egbert, G.D.; Erofeeva, G.D. Effective Inverse Modeling of Barotropic Ocean Tides. *J. Atmos. Ocean. Technol.* **2002**, *19*, 183–204. [CrossRef]

24. Warner, J.C.; Sherwood, C.R.; Signell, R.P.; Harris, C.K.; Arango, H.G. Development of a three-dimensional, regional, coupled wave, current, and sediment-transport model. *Comput. Geosci.* **2008**, *34*, 1284–1306. [CrossRef]

25. Le Tuan, A.N.H.; Anh, D.H.; Linh, M.T.Y.; Thao, N.D. Investigation typhoon induced storm surge and high wave in Vietnam using coupled Delft3d-FLOW–WAVE models combined with weather research forecast (WRF) output wind field. *Vnuhcm J. Eng. Technol.* **2021**, *4*, 645–662.

26. Skamarock, W.C.; Klemp, J.B.; Dudhia, J.; Gill, D.O.; Barker, D.M.; Duda, M.G.; Huang, X.Y.; Wang, W.; Powers, J.G. *A Description of the Advanced Research WRF Version 3*; Technical Report; National Center for Atmospheric Research: Boulder, CO, USA, 2008.

27. De Tomasi, F.; Martano, P.; Miglietta, M.; Morabito, A.; Perrone, M.R. Lidar monitoring of water vapor and comparison with numerical simulations. *Nuovo C. Soc. Ital. Di Fis. Sez. C* **2003**, *26*, 373–386.

28. Fedele, F.; Tateo, A.; Menegotto, M.; Turnone, A.; Figorito, B.; Carducci, A.G.C.; Calculli, C.; Ribecco, N.; Pollice, A.; Bellotti, R. Impact of Planetary Boundary Layer parametrization scheme and land cover classification on surface processes: Wind speed and temperature bias spatial distribution analysis over south Italy. In Proceedings of the 15th EMS Annual Meeting & 12th European Conference on Applications of Meteorology (ECAM), Sofia, Bulgaria, 7–11 September 2015.

29. Fedele, F.; Miglietta, M.M.; Perrone, M.R.; Burlizzi, P.; Bellotti, R.; Conte, D.; Carducci, A.G.C. Numerical simulations with the WRF model of water vapour vertical profiles: A comparison with LIDAR and radiosounding measurements. *Atmos. Res.* **2015**, *166*, 110–119. [CrossRef]

30. Berman, F.; Chien, A.; Cooper, K.; Dongarra, J.; Foster, I.; Gannon, D.; Johnsson, L.; Kennedy, K.; Kesselman, C.; Mellor-Crumme, J.; et al. The GrADS project: Software support for high-level grid application development. *Int. J. High. Perform. Comput. Appl.* **2001**, *15*, 327–344. [CrossRef]

31. Iriza, A.; Dumitrache, R.C.; Lupascu, A.; Stefan, S. Studies regarding the quality of numerical weather forecasts of the WRF model integrated at high-resolutions for the Romanian territory. *Atmósfera* **2016**, *29*, 11–21. [CrossRef]

32. Yesubabu, V.; Kattamanchi, V.K.; Vissa, N.K.; Dasari, H.P.; Sarangam, V.B.R. Impact of ocean mixed-layer depth initialization on the simulation of tropical cyclones over the Bay of Bengal using the WRF-ARW model. *Meteorol. Appl.* **2019**, *27*, e1862. [CrossRef]

33. Shahi, N.K.; Polcher, J.; Bastin, S.; Pennel, R.; Fita, L. Assessment of the spatio-temporal variability of the added value on precipitation of convection-permitting simulation over the Iberian Peninsula using the RegIPSL regional earth system model. *Clim. Dyn.* **2022**, *59*, 471–498. [CrossRef]

34. Tateo, A.; Campanaro, V.; Amoroso, N.; Bellantuono, L.; Monaco, A.; Pantaleo, E.; Rinaldi, R.; Maggipinto, T. Predicting Air Quality from Measured and Forecast Meteorological Data: A Case Study in Southern Italy. *Atmosphere* **2023**, *14*, 475. [CrossRef]

35. Tateo, A.; Miglietta, M.M.; Fedele, F.; Menegotto, M.; Monaco, A.; Bellotti, R. Ensemble using different Planetary Boundary Layer schemes in WRF model for wind speed and direction prediction over Apulia region. *Adv. Sci. Res.* **2017**, *14*, 95–102. [CrossRef]